NJC

ROYAL SOCIETY OF CHEMISTRY

COMMUNICATION

View Article Online
View Journal

Cite this: DOI: 10.1039/d6nj01950a

Received 26th May 2026,
Accepted 26th May 2026

DOI: 10.1039/d6nj01950a

rsc.li/njc

Alkane dehydrogenation catalyzed by a PN^{3}P pincer iridium hydride complex

Kher Ai Chiaw,[a] Suma Basappa,[b] Manoj V. Mane,[b] Kuo-Wei Huang,*[c] Nicholas Long*[d] and Sandeep Suryabhan Gholap*[a]

The use of an iridium-based pincer complex, specifically the PN^{3}P pincer ligand backbone, for an efficient alkane dehydrogenation reaction is explored. Herein, we investigate the catalytic performance of a PN^{3}P pincer iridium dihydride complex (Ir2) in the dehydrogenation reaction of cyclooctane to cyclooctene. With 0.1 mol% of Ir2, cyclooctane with *tert*-butylethylene (TBE) as a hydrogen acceptor and NaO^{t}Bu as a base, we achieved conversion up to 55% of *tert*-butylethylene (TBE) with a TON up to 546. These results highlight the potential of PN^{3}P pincer iridium dihydride complexes as robust catalysts for selective alkane dehydrogenation under mild reaction conditions. Furthermore, DFT calculations strongly support our proposed mechanism.

Alkane dehydrogenation (AD) is one of the most important reactions in the petrochemical industry as it uses abundant alkane to produce valuable olefins that are chemically versatile and can act as intermediates in higher value alkane synthesis through olefin coupling.[1,2] This reaction can also serve as an alternative pathway for high-temperature steam cracking of alkanes, which is energy-consuming and produces several undesirable side-products.[3] In the case of alkane dehydrogenation, molecular hydrogen (H_2) is produced as the primary by-product along with olefins. H_2 is one of the rising energy carriers owing to its high energy density and environmentally benign nature.[4] While significant efforts have been devoted to hydrogen production, such as *via* water splitting,[5a] methane pyrolysis[5b] and biomass gasification,[5c] AD could eventually also serve as an attractive alternative pathway for H_2 generation. Despite the attractive advantages of the dehydrogenation of alkanes to alkenes and H_2, it is a highly endothermic process,[6] and this characteristic is a serious hindrance to the wide implementation of this reaction.

There are some examples of metal complexes developed over the past few decades for the dehydrogenation of alkanes, including those used with hydrogen acceptors, UV and irradiation.[7,8] However, those complexes that contain a PCP pincer-type ligand utilized with a hydrogen acceptor have emerged at the top, outperforming the others in terms of stability, TON and selectivity.[2,9] Pincer ligands incorporating iridium are often used in catalytic dehydrogenation systems given their outstanding catalytic activity and stability.[7,10–15] Over the past decade, the high-valent oxidation state of iridium has been extensively explored for the catalytic dehydrogenation of alkanes.[16–23]

Early work by Jensen and Kaska in 1996 demonstrated the potential of such systems.[16a] They first synthesized complex **2** from **1** in the presence of H_2 and $LiBEt_3H$ (Scheme 1), where the iridium dihydride complex **2** showed greater stability with no observable decomposition over a week; whereas the hydrochloride precursor **1** showed significant decomposition after 24 h. These foundational studies have established the basis of pincer–iridium catalysts, enabling further detailed mechanistic investigations on this catalytic system.

In 2021, Goldmann and co-worker reported alkane dehydrogenation catalysed by a (^{t}Bu$_4$POCOP)Ir complex that proceeded

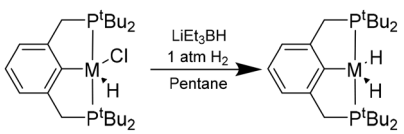

Scheme 1 Iridium dihydride complex developed by Jensen and Kaska for the dehydrogenation of alkanes.

[a] *Institute of Sustainability for Chemical, Energy and Environment (ISCE^2), Agency of Science, Technology and Research (A*STAR), 1 Pesek Road, Jurong Island, Singapore 627833, Singapore. E-mail: sandeep_gholap@a-star.edu.sg*
[b] *Centre for Nano and Material Sciences, Jain (Deemed-to-be University), Bangalore, Karnataka 562112, India*
[c] *Center for Renewable Energy and Storage Technologies, KAUST Catalysis Platform, and Division of Physical Science and Engineering, King Abdullah University of Science and Technology, Thuwal, 23955-6900, Saudi Arabia. E-mail: hkw@kaust.edu.sa*
[d] *Department of Chemistry, Imperial College London, White City Campus, London, W12 0BZ, UK. E-mail: n.long@imperial.ac.uk*

through a proton-coupled electron-transfer (PCET) pathway using oxidants and bases as a proton and electron acceptor.[24] In a subsequent study, they investigated the intramolecular C(sp^3)–H activation during alkane dehydrogenation using (*p*-pyridyl-^{t}BuPCP)–IrCl$^+$ cation (*p*-pyridyl-^{t}BuPCP = 3,5-*bis*(di-tert-butylphosphinomethyl)-2,6-dimethylpyridin-4-yl) complexes.[25] In 2022, the same group further expanded this chemistry by reporting a bis(2-di-*tert*-butyl-phosphinophenyl)phosphine (^{t}BuP^HPP) iridium complex for the dehydrogenation of alkanes and demonstrated that the C–H activation using a more crowded Ir(III) complex (^{t}Bu$_4$PCP)IrCl$^+$ (^{R}PCP = 2,6-C$_6$H$_3$(CH$_2$PR$_2$) occurred intramolecularly, whereas the less crowded (^{i}Pr$_4$PCP)IrCl$^+$ undergoes intermolecular C–H activation.[9,19]

Metal–ligand cooperativity (MLC) plays an important role in C–H bond activation by enabling reversible ligand participation during catalysis.[26–33] In the case of a pyridine-based pincer complex, the MLC involved in the aromatization–dearomatization of the pyridine ring results in more efficient activation of various bonds.[29,34–51] PN^{3}P pincer complexes have previously demonstrated great performance in various chemical reactions, particularly in CO_2 hydrogenation[52] and formic acid dehydrogenation.[53] Herein, we report the catalytic activity of a PN^{3}P–pincer iridium complex towards the dehydrogenation of alkanes (Fig. 1) and the evaluation of PN^{3}P–pincer iridium complexes **Ir1**, **Ir2** and **Ir3** for alkane dehydrogenation (Table 1).

To continue the study of these PN^{3}P–pincer iridium complexes, we synthesized **Ir1**, **Ir2** and **Ir3** according to a previously reported method.[54] To test the performance of these catalysts for dehydrogenation reactions, we investigated the dehydrogenation reaction of cyclooctane (COA) as a model substrate and *tert*-butylethylene (TBE) as a sacrificial hydrogen acceptor. We conducted the reaction of cyclooctane (3.0 mmol) and TBE (3.0 mmol) with sodium *tert*-butoxide (NaO^{t}Bu) as a base and an **Ir1** catalyst (3.0 μmol, 0.1 mol%). The reaction mixture was heated at 150 °C in a closed reaction tube. The reaction was monitored by GC-MS as well as ^{1}H-NMR, and we observed after 24 h the formation of cyclooctene (COE) as well as a trace amount of the 1,3-cyclooctadiene (1,3-COD) product with an overall conversion of 10%, and a TON up to 99 was achieved (Table 1, entry 1). Next, we studied the performance of the dearomatized PN^{3}P pincer dihydride iridium complex, **Ir2**. Surprisingly, the **Ir2** catalyst under similar reaction conditions gave 55% conversion with a TON up to 546 (Table 1, entry 2). When the **Ir3** catalyst was tested under similar reaction conditions, it gave a conversion of 40% with a TON up to 403 (Table 1, entry 3). Next, we studied the effect of oxidants to tune the oxidation potential, for example ferrocenium salts, $[Fe]^+[BF_4]^-$, for alkane dehydrogenation reactions.[24] We observed that the addition of $[Fe]^+[BF_4]^-$ salt (Fe = Ferrocenium) to the reaction mixture enhanced the conversion for all Ir catalysts by 2–6% (Table 1, entries 4–6). Next, we examined the effect of another base, namely potassium *tert*-butoxide (KO^{t}Bu), with and without adding $[Fe]^+[BF_4]^-$, which gives a slightly lower conversion as compared to NaO^{t}Bu (Table 1, entries 7 and 8).

The concentration of TBE also plays a crucial role in driving the dehydrogenation reaction of COA forward. We studied different ratios of **Ir2**:TBE:COA as shown in Table 2. When the reaction was carried out with a ratio of 1 : 100 : 1000 of **Ir2**:TBE:COA, it resulted in 5% conversion with a TON up to 3 (Table 2, entry 1). The conversion for the dehydrogenation of COA was increased to 24% when the ratio of TBE was increased to 1 : 500 : 1000, giving a TON up to 118 (Table 2, entry 2). On further increase of the ratio to 1 : 1000 : 1000, the conversion enhanced to 55% with a higher TON of up to 546 (Table 2, entry 3). This observation highlights the importance of maintaining a sufficiently high molar ratio of TBE to COA to effectively scavenge hydrogen and shift the reaction equilibrium towards dehydrogenation.

Table 1 Optimization of the reaction conditions towards cyclooctane dehydrogenation[a]

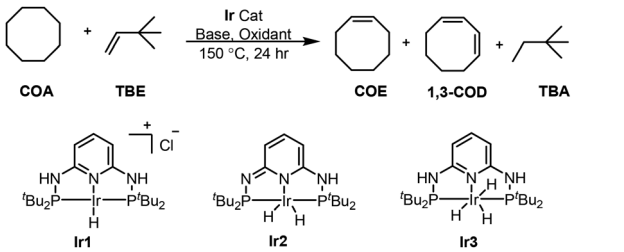

Entry	Ir cat.	Base	Oxidant	Conv.[b] (%)	TON[b]
1	**Ir1**	NaO^{t}Bu	—	10	99
2	**Ir2**	NaO^{t}Bu	—	55	546
3	**Ir3**	NaO^{t}Bu	—	40	403
4	**Ir1**	NaO^{t}Bu	$[Fe]^+[BF_4]^-$	16	157
5	**Ir2**	NaO^{t}Bu	$[Fe]^+[BF_4]^-$	56	558
6	**Ir3**	NaO^{t}Bu	$[Fe]^+[BF_4]^-$	42	415
7	**Ir2**	KO^{t}Bu	—	48	481
8	**Ir2**	KO^{t}Bu	$[Fe]^+[BF_4]^-$	50	502

[a] For the reaction, alkane (3.0 mmol), TBE (3.0 mmol), **Ir cat** (3.0 μmol, 0.1 mol%), base (15.0 μmol, 0.5 mol%), and oxidant (15.0 μmol, 0.5 mol%) were heated in an autoclave. [b] Determined by GC using mesitylene as an internal standard. TONs were calculated based on conversion of TBE determined by GC.

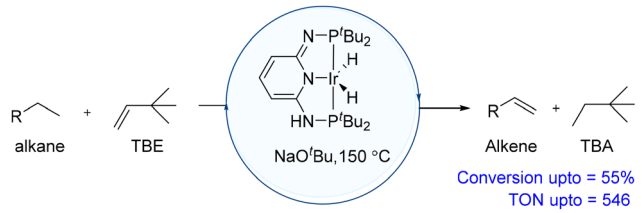

Fig. 1 This work: alkane dehydrogenation catalysed by a PN^{3}PIrH$_2$ complex.

Table 2 Optimization of the reaction conditions towards cyclooctane dehydrogenation[a]

Entry	[Ir]:COA	[Ir]:TBE	Temp.	Conv.[b] (%)	TON[b]
1	1000	100	150	5	3
2	1000	500	150	24	118
3	1000	1000	150	55	546

[a] For the reaction, alkane (3.0 mmol), TBE (0.3–3.0 mmol), **Ir2 cat** (0.1 mol%), and NaO^{t}Bu (15.0 μmol, 0.5 mol%) were heated in an autoclave. [b] Determined by GC using mesitylene as an internal standard. TON was calculated based on the conversion of TBE determined by GC.

Further, we explored the dehydrogenation process with KO^{t}Bu and NaO^{t}Bu as a base at different time intervals. In the case of KO^{t}Bu, the reaction was carried out initially for 4 h, and GC analysis of the reaction mixture showed a TBE conversion of 45% with a TON of up to 447 (Table 3, entry 1). Extending the reaction time to 16 h and 24 h further increased the TBE conversion to 47% and 48%, respectively, with a corresponding TON up to 466 and 481 (Table 3, entries 2 and 3). Whereas, in the case of NaO^{t}Bu as a base, 4 h, 16 h and 24 h time intervals gave 49%, 50% and 55% TBE conversion with a TON up to 499, 501 and 546, respectively (Table 3, entries 4–6). This observation suggested that extending the reaction time for the dehydrogenation reaction does not substantially improve the catalytic activity of **Ir2**.

Next, we studied the substrate scope using both linear and cyclic alkanes. The dehydrogenation of linear alkanes is particularly challenging because of the higher energy required for C–H activation compared to cyclic alkanes.[55] We initially explored *n*-octane as a substrate. The reaction was carried out using *n*-octane, **Ir2**, and NaO^{t}Bu in the presence of TBE at 150 °C. After 15 h reaction time, the reaction was analyzed by GC, which gave 15% TBE conversion. Along with 1-octene as the dehydrogenated product, we also observed a trace amount of isomerized 2-octene and 1,2-dimethylcyclohexane (Table 4, entry 1). These results suggest that the linear alkane shows lower reactivity towards the dehydrogenation reaction. In contrast, a cyclic alkane, namely cyclohexane, is effectively converted to cyclohexene with a yield of 10% (Table 4, entry 2). However, complete dehydrogenation of the product to form benzene was not observed. Next, we evaluated 1,2,3,4-tetrahydronaphthalene as a bicyclic substrate. After the reaction, we observed fully dehydrogenated naphthalene as a product with 25% total conversion along with 5% of the partially dehydrogenated product, 1,4-dihydronapthalene (Table 4, entry 3).

To shed light on the reaction mechanism, density functional theory (DFT) calculations were performed using the Gaussian 16 suite[56] (for more details, see the supplementary information (SI)). As shown in Fig. 2, the reaction cycle begins with the formation of catalytically active species **IN1**, resulting from the reaction of **Ir2** with the base NaO^{t}Bu along with the loss of ^{t}BuOH. The active species **IN1** then forms a loosely bound adduct with TBE to form **IN2**, which is uphill by 5.7 kcal mol^{-1}. Next, the first hydrogen abstraction occurs at **IN2** to give **IN3** *via* three membered transition state **TS1**, with a free energy barrier of 29.7 kcal mol^{-1}. Subsequently, **IN3** undergoes the second hydrogen abstraction to generate the Ir-catalyst (**IN4**) in its lowest oxidation state along with the alkane, having a transition state (**TS2**) barrier of 6.5 kcal mol^{-1}. Then, the complex **IN4** binds with the cyclooctane *via* σ-complex **IN5**, which is slightly exergonic by 3.9 kcal mol^{-1}. Next, **IN5** undergoes 1,2-addition of the C–H bond across the Ir catalyst to give cyclooctane intermediate **IN6**, traversing transition state **TS3** with a barrier of 10.2 kcal mol^{-1}. Finally, the β-hydride abstraction from the cyclooctyl group in **IN7** leads to the formation of the cyclooctene product (**COE**) along with the regeneration of active catalyst **IN1**. These four membered transition states (TS4) required a transition state barrier of 11.8 kcal mol^{-1}. Overall, these calculations indicate that the alkene insertion is the rate

Table 3 Time-dependent study for cyclooctane dehydrogenation[a]

Entry	Time (h)	Base	Conv. of TBE[b] (%)	TON[b]
1	4	KO^{t}Bu	45	447
2	16	KO^{t}Bu	47	466
3	24	KO^{t}Bu	48	481
4	4	NaO^{t}Bu	49	499
5	16	NaO^{t}Bu	50	501
6	24	NaO^{t}Bu	55	546

[a] For the reaction, alkane (3.0 mmol), TBE (3.0 mmol), **Ir2 cat** (0.1 mol %), and base (15.0 μmol, 0.5 mol%) were heated in an autoclave. [b] Determined by GC using mesitylene as an internal standard. TON was calculated based on conversion of TBE determined by GC.

Table 4 Substrate scope study[a]

Entry	Alkane	Product	Conv.[b] (%)
1	*n*-octane	1-octene (7%) + 4% + 2-octene (4%)	15
2		+ not observed	10
3		20% + 5%	25

[a] For the reaction, alkane (3.0 mmol), TBE (3.0 mmol), **Ir2 cat** (0.1 mol %), and NaO^{t}Bu (15.0 μmol, 0.5 mol%) were heated in an autoclave. [b] Determined by GC using mesitylene as an internal standard.

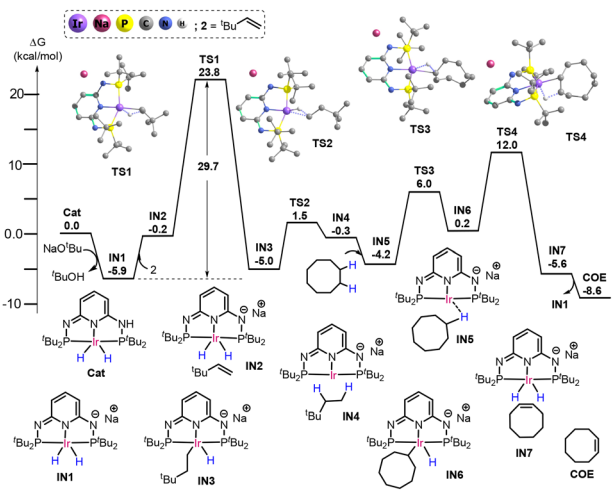

Fig. 2 Free energy profile of the dehydrogenation of cyclooctane using an **Ir2** catalyst. Free energy values are at the M06/SDD(Ir)/def2-TZVP(C,H,O,N,P,Na)//BP86/SDD(Ir)/def2-SVP(C,H,O,N,P,Na) level of theory. Non-essential hydrogen atoms have been omitted for the sake of clarity.

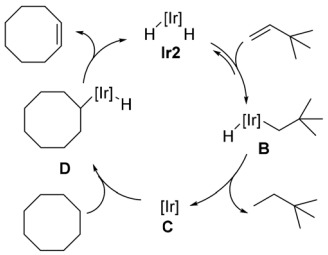

Fig. 3 Possible reaction mechanism of COA with TBE using **Ir2**.

determining step of the reaction with the highest transition energy barrier of 29.7 kcal mol^{-1}.

After the detailed DFT study, the possible reaction mechanism is illustrated as shown in Fig. 3.[57] The first step is the insertion of TBE into the 16-electron iridium dihydride (**Ir2**) complex to produce alkyl hydride complex B, which undergoes reductive elimination to form the 14-electron C species. This complex activates the C–H bond of cyclooctane to give species D, followed by β-hydride elimination to yield cyclooctene and regenerate the **Ir2**.

Conclusion

PN^3P iridium complexes **Ir1**, **Ir2** and **Ir3** with 2,6-diamino phosphine ligands have been studied towards the dehydrogenation of alkanes. The PN^3P pincer iridium dihydride complex (**Ir2**) shows good catalytic performance in the dehydrogenation reaction of cyclooctane to cyclooctene. We achieved conversion up to 55% of *tert*-butylethylene (TBE) with a TON up to 546. These results highlight the potential of the PN^3P pincer iridium dihydride complex as a robust catalyst for selective alkane dehydrogenation under mild reaction conditions. DFT calculations show that once the active species **I** formed after the treatment of NaO^tBu, it forms a loosely bound adduct with TBE to form intermediate **II**, which is uphill by 5.7 kcal mol^{-1}. Given that TBE is a mono substituted olefin and highly selective for hydrogenation, the dehydrogenation is turnover-limiting and alkene (TBE and COE) complexes are the resting states. When the concentration of TBE is low, the hydrogenation is turnover-limiting and the resting state is **Ir2**, while at high [TBE], COA dehydrogenation is turnover-limiting, and the resting state is the vinyl hydride.

Conflicts of interest

The authors declare no competing financial interest.

Data availability

The authors confirm that the data supporting the findings of this study are available within the article and its supplementary information. Raw data that support the findings of the study are available from the corresponding author, upon reasonable request. Supplementary information is available. See DOI: https://doi.org/10.1039/d6nj01950a.

Acknowledgements

This work was supported by the Agency for Science, Technology and Research's (A*STAR) Council Strategic Fund C230415018 and the HTCO Seed Fund (C231218002). M. V. M. is thankful for the financial support from the ANRF (ANRF/ECRG/2024/002337/CS) and CNMS, Jain University, Bangalore, India. H. K. W. acknowledge King Abdullah University of Science and Technology (KAUST).

References

1 J. A. Labinger, D. C. Leitch, J. E. Bercaw, M. A. Deimund and M. E. Davis, *Top. Catal.*, 2015, **58**, 494–501.
2 K. I. Goldberg and A. S. Goldman, *Acc. Chem. Res.*, 2017, **50**, 620–626.
3 (*a*) S. J. F. Sadrameli, *Acc. Chem. Res.*, 2015, **140**, 102–115; (*b*) T. Ren, M. Patel and K. Blok, *Energy*, 2006, **31**, 425–451; (*c*) M. Tuomaala, M. Hurme and A. M. Leino, *Appl. Therm. Eng.*, 2010, **30**, 45–52.
4 K. Mazloomi and C. Gomes, *Renewable Sustainable Energy Rev.*, 2012, **16**, 3024–3033.
5 (*a*) G. Chen and T. Zhang, *cMat*, 2025, **2**, e12287; (*b*) S. R. Patlolla, K. Katsu, A. Sharafian, K. Wei, O. E. Herrera and W. Mérida, *Renewable Sustainable Energy Rev.*, 2023, **181**, 113323; (*c*) A. C. Chang, H. F. Chang, F. J. Lin, K. H. Lin and C. H. Chen, *Int. J. Hydrogen Energy*, 2011, **36**, 14252–14260.
6 H. Afeefy, NIST Chemistry Webook 2005.
7 (*a*) A. Kumar, T. M. Bhatti and A. S. Goldman, *Chem. Soc. Rev.*, 2017, **117**, 12357–12384; (*b*) J. J. Sattler, J. Ruiz-Martinez, E. Santillan-Jimenez and B. M. Weckhuysen, *Chem. Rev.*, 2014, **114**, 10613–10653; (*c*) Z. Nawaz, *Rev. Chem. Eng.*, 2015, **31**, 413–436.
8 (*a*) M. J. Burk and R. H. Crabtree, *J. Am. Chem. Soc.*, 1987, **109**, 8025–8032; (*b*) D. Shee and A. Sayari, *Appl. Catal., A*, 2010, **389**, 155–164.
9 B. M. Gordon, N. Lease, T. J. Emge, F. Hasanayn and A. S. Goldman, *J. Am. Chem. Soc.*, 2022, **144**, 4133–4146.
10 (*a*) X. Jia and Z. Huang, *Nat. Chem.*, 2016, **8**, 157–161; (*b*) F. Yu, R. Tao, Y. Su, G. Liu and Z. Huang, *Org. Lett.*, 2022, **24**, 4563–4568.
11 R. H. Crabtree, M. F. Mellea, J. M. Mihelcic and J. M. Quirk, *J. Am. Chem. Soc.*, 1982, **104**, 107–113.
12 M. J. Burk, R. H. Crabtree, C. P. Parnell and R. J. Uriarte, *Organometallics*, 1984, **3**, 816–817.
13 M. Findlater, J. Choi, A. S. Goldman and M. Brookhart, *Catal. Met. Complexes*, Springer, 2012, pp. 113–141.
14 J. Choi, A. H. R. MacArthur, M. Brookhart and A. S. Goldman, *Chem. Rev.*, 2011, **111**, 1761–1779.
15 M. C. Haibach, S. Kundu, M. Brookhart and A. S. Goldman, *Acc. Chem. Res.*, 2012, **45**, 947–958.
16 (*a*) M. Gupta, C. Hagen, R. J. Flesher, W. C. Kaska and C. M. Jensen, *Chem. Commun.*, 1996, 2083–2084; (*b*) M. Gupta, C. Hagen, R. J. Flesher, W. C. Kaska and C. M. Jensen, *Chem. Commun.*, 1996, 2083–2084; (*c*) J. Belli and C. M. Jensen, *Organometallics*, 1996, 1532–1534; (*d*) M. Gupta, C. Hagen,

W. C. Kaska, R. E. Cramer and C. M. Jensen, *J. Am. Chem. Soc.*, 1997, **119**, 840–841; (*e*) D. W. Lee, W. C. Kaska and C. M. Jensen, *Organometallics*, 1998, **17**, 1–3; (*f*) C. M. Jensen, *Chem. Commun.*, 1999, 2443–2449; (*g*) D. Morales-Morales, D. W. Lee, Z. Wang and C. M. Jensen, *Organometallics*, 2001, **20**, 1144–1147; (*h*) D. Morales-Morales, R. Redón, C. Yung and C. M. Jensen, *Inorg. Chim. Acta*, 2004, **357**, 2953–2956.

17 (*a*) K. B. Renkema, Y. V. Kissin and A. S. Goldman, *J. Am. Chem. Soc.*, 2003, **125**, 7770–7771; (*b*) K. E. Allen, D. M. Heinekey, A. S. Goldman and K. I. Goldberg, *Organometallics*, 2013, **32**, 1579–1582.

18 (*a*) X. Zhou, S. Malakar, T. Dugan, K. Wang, A. Sattler, D. O. Marler, T. J. Emge, K. Krogh-Jespersen and A. S. Goldman, *ACS Catal.*, 2021, **11**, 14194–14209; (*b*) A. Parihar, T. J. Emge, F. Hasanayn and A. S. Goldman, *J. Am. Chem. Soc.*, 2025, **147**, 10279–10297.

19 S. Kundu, Y. Choliy, G. Zhuo, R. Ahuja, T. J. Emge, R. Warmuth, M. Brookhart, K. Krogh-Jespersen and A. S. Goldman, *Organometallics*, 2009, **28**, 5432–5444.

20 A. Kumar, T. Zhou, T. J. Emge, O. Mironov, R. J. Saxton, K. Krogh-Jespersen and A. S. Goldman, *ACS Catal.*, 2015, **137**, 9894–9911.

21 R. Ahuja, B. Punji, M. Findlater, C. Supplee, W. Schinski, M. Brookhart and A. S. Goldman, *Nat. Chem.*, 2011, **3**, 167–171.

22 B. Punji, T. J. Emge and A. S. Goldman, *Organometallics*, 2010, **29**, 2702–2709.

23 A. Paul and C. B. Musgrave, *Angew. Chem., Int. Ed.*, 2007, **46**, 8153.

24 A. D. R. Shada, A. J. Miller, T. J. Emge and A. S. Goldman, *ACS Catal.*, 2021, **11**, 3009–3016.

25 T. M. Bhatti, A. Kumar, A. Parihar, H. K. Moncy, T. J. Emge, K. M. Waldie, F. Hasanayn and A. S. Goldman, *J. Am. Chem. Soc.*, 2023, **145**, 18296–18306.

26 D. Milstein, *Philos. Trans. R. Soc., A*, 2015, **373**, 20140189.

27 M. Rauch, S. Kar, A. Kumar, L. Avram, L. J. Shimon and D. Milstein, *J. Am. Chem. Soc.*, 2020, **142**, 14513–14521.

28 J. R. Khusnutdinova and D. Milstein, *Angew. Chem., Int. Ed.*, 2015, **54**, 12236–12273.

29 T.-F. Ramspoth, J. Kootstra and S. R. Harutyunyan, *Chem. Soc. Rev.*, 2024, **53**, 3216–3223.

30 N. E. Smith, W. H. Bernskoetter and N. Hazari, *J. Am. Chem. Soc.*, 2019, **141**, 17350–17360.

31 M. R. Elsby and R. T. Baker, *Chem. Soc. Rev.*, 2020, **49**, 8933–8987.

32 E. Ben-Ari, G. Leitus, L. J. Shimon and D. Milstein, *J. Am. Chem. Soc.*, 2006, **128**, 15390–15391.

33 (*a*) E. Fogler, J. A. Garg, P. Hu, G. Leitus, L. J. Shimon and D. Milstein, *Chem. – Eur. J.*, 2014, **20**, 15727–15731; (*b*) Q.-Q. Zhou, Y.-Q. Zou, S. Kar, Y. Diskin-Posner, Y. Ben-David and D. Milstein, *ACS Catal.*, 2021, **11**, 10239–10245.

34 C. Gunanathan and D. Milstein, *Acc. Chem. Res.*, 2011, **44**, 588–602.

35 H. Li, B. Zheng and K.-W. Huang, *Coord. Chem. Rev.*, 2015, **293**, 116–138.

36 T. Shimbayashi and K. I. Fujita, *Catalysts*, 2020, **10**, 635.

37 T. Zell and D. Milstein, *Acc. Chem. Res.*, 2015, **48**, 1979–1994.

38 T. P. Gonçalves, I. Dutta and K.-W. Huang, *Chem. Commun.*, 2021, **57**, 3070–3082.

39 Y. Pan, C. L. Pan, Y. Zhang, H. Li, S. Min, X. Guo, B. Zheng, H. Chen, A. Anders and Z. Lai, *Chem. – Asian J.*, 2016, **11**, 1357–1360.

40 M. H. Huang, J. Hu and K.-W. Huang, *J. Chin. Chem. Soc.*, 2018, **65**, 60–64.

41 H. Li, Y. Wang, Z. Lai and K.-W. Huang, *ACS Catal.*, 2017, **7**, 4446–4450.

42 T. Chen, H. Li, S. Qu, B. Zheng, L. He, Z. Lai, Z.-X. Wang and K.-W. Huang, *Organometallics*, 2014, **33**, 4152–4155.

43 S. S. Gholap, A. Al Dakhil, P. Chakraborty, H. Li, I. Dutta, P. K. Das and K.-W. Huang, *Chem. Commun.*, 2021, **57**, 11815–11818.

44 S. B. Dawood, P. Chakraborty, L. Yang and K.-W. Huang, *Tetrahydron Lett.*, 2025, **167**, 155664.

45 Y. Pan, C. L. Pan, Y. Zhang, H. Li, S. Min, X. Guo, B. Zheng, H. Chen, A. Anders and Z. Lai, *Chem. – Asian J.*, 2016, **11**, 1294.

46 M. J. Ajitha and K.-W. Huang, *Organometallics*, 2025, **44**, 2099–2106.

47 S. Qu, Y. Dang, C. Song, M. Wen, K.-W. Huang and Z.-X. Wang, *J. Am. Chem. Soc.*, 2014, **136**, 4974–4991.

48 H. Li, T. P. Gonçalves, D. Lupp and K.-W. Huang, *ACS Catal.*, 2019, **9**, 1619–1629.

49 T. P. Gonçalves and K.-W. Huang, *J. Am. Chem. Soc.*, 2017, **139**, 13442–13449.

50 C. Guan, Y. Pan, E. P. L. Ang, J. Hu, C. Yao, M.-H. Huang, H. Li, Z. Lai and K.-W. Huang, *Green Chem.*, 2018, **20**, 4201–4205.

51 L.-P. He, T. Chen, D.-X. Xue, M. Eddaoudi and K.-W. Huang, *J. Organomet. Chem.*, 2012, **700**, 202–206.

52 Y. Pan, C. Guan, H. Li, P. Chakraborty, C. Zhou and K.-W. Huang, *Dalton Trans.*, 2019, **48**, 12812–12816.

53 L. Alrais, S. S. Gholap, I. Dutta, E. Abou-Hamad, B. W. J. Chen, J. Zhang, M. N. Hedhili, J.-M. Basset and K.-W. Huang, *Appl. Catal., B*, 2024, **342**, 123439.

54 Y. Pan, C. Guan, H. Li, P. Chakraborty, C. Zhou and K.-W. Huang, *Dalton Trans.*, 2019, **48**, 12812–12816.

55 X. Tang, X. Jia and Z. Huang, *Chem. Sci.*, 2018, **9**, 288–299.

56 M. Frisch, *et al.*,. *Gaussian 16, Revision C.02*, Gaussian, Inc., Wallingford CT, 2019.

57 D. Bézier, C. Guan, K. Krogh-Jespersen, A. S. Goldman and M. J. Brookhart, *Chem. Sci.*, 2016, **7**, 2579–2586.